scientific reports

Check for updates

OPEN

Automatic CTA analysis for blood vessels and aneurysm features extraction in EVAR planning

Erich Robbi[1]✉, Daniele Ravanelli[2], Sara Allievi[3], Igor Raunig[3], Stefano Bonvini[3], Andrea Passerini[1] & Annalisa Trianni[2]

Endovascular Aneurysm Repair (EVAR) is a minimally invasive procedure crucial for treating abdominal aortic aneurysms (AAA), where precise pre-operative planning is essential. Current clinical methods rely on manual measurements, which are time-consuming and prone to errors. Although AI solutions are increasingly being developed to automate aspects of these processes, most existing approaches primarily focus on computing volumes and diameters, falling short of delivering a fully automated pre-operative analysis. This work presents BRAVE (Blood Vessels Recognition and Aneurysms Visualization Enhancement), the first comprehensive AI-driven solution for vascular segmentation and AAA analysis using pre-operative CTA scans. BRAVE offers exhaustive segmentation, identifying both the primary abdominal aorta and secondary vessels, often overlooked by existing methods, providing a complete view of the vascular structure. The pipeline performs advanced volumetric analysis of the aneurysm sac, quantifying thrombotic tissue and calcifications, and automatically identifies the proximal and distal sealing zones, critical for successful EVAR procedures. BRAVE enables fully automated processing, reducing manual intervention and improving clinical workflow efficiency. Trained on a multi-center open-access dataset, it demonstrates generalizability across different CTA protocols and patient populations, ensuring robustness in diverse clinical settings. This solution saves time, ensures precision, and standardizes the process, enhancing vascular surgeons' decision-making.

Keywords Abdominal aortic aneurysm, Artificial intelligence, CT angiography, Endovascular aneurysm repair, Planning process

Endovascular Aneurysm Repair (EVAR) has become the primary treatment option for Abdominal Aortic Aneurysm (AAA) in suitable patients over the last decade, due to its lower perioperative morbidity and mortality compared with the open approach[1,2]. EVAR isolates the AAA using a stent-graft (SG) with three sealing zones: one at the aorta and two at the common iliac arteries, ensuring secure attachment and diverting blood flow from the aneurysmal sac to prevent rupture. Precise imaging is a key component of the care pathway for patients with AAA. Contrast-enhanced computed tomography angiography (CTA) analysis with dedicated workstations allows for a 3D evaluation of the complete aortic anatomy, essential for accurate measurements[3].

EVAR feasibility relies on assessing morphological characteristics of the aorta, AAA sac and surrounding anatomy from pre-operative CTA (pre-CTA). These characteristics are crucial for optimal SG sizing, accurate EVAR planning and for determining the quality of arterial access points for SG deployment. Recently, the new ESVS guidelines 2024[2] propose the EVAR sizing and planning worksheet, which outlines the key morphological features that vascular surgeons need to measure. These include, among others, the location of the renal artery, to ensure the SG does not block renal flow, and the diameter, length, and angulation of the proximal neck, to ensure proper seal and fixation of the SG.

All the anatomic features for EVAR eligibility are typically evaluated by the vascular surgeons using dedicated commercial image processing software for EVAR sizing. However, this task is challenging, requires a long learning curve, and remains operator-dependent and time-consuming, particularly in the presence of aberrant anatomy, tortuous aorta and significant disease around the lumen[4]. This process might be complex for everyday clinical practice, even with advanced 3D workstations, and results are affected by high inter- and intra-operator

[1]Department of Information Engineering and Computer Sciences, DISI of University of Trento, Via Sommarive, Trento 38123, Italy. [2]Medical Physics Department of Provincial Agency for Health Services of the Autonomous Province of Trento, APSS, S. Chiara Hospital, Trento 38121, Italy. [3]Vascular Surgery Department of Provincial Agency for Health Services of the Autonomous Province of Trento, APSS, S. Chiara Hospital, Trento 38121, Italy. ✉email: erich.robbi@unitn.it

variability.[4] Moreover, some parameters, such as AAA body volume, AAA lumen volume, and thrombus volume, are not directly provided by all clinical software[5,6].

Traditional analytical approaches, such as active contour and morphological snake models[7], have been used to overcome the limitations of manual segmentation, with promising results in the automatic segmentation of both the aortic lumen and intraluminal thrombus. The advent of AI in research has further enhanced these efforts, with AI-based solutions, such as deep neural networks[6,8–15], demonstrating significant potential.

Despite significant breakthroughs, most research to date has primarily focused on AAA thrombus segmentation and the automated measurement of a limited subset of the morphological features necessary for EVAR planning. Recently some studies focused their attention on automatic segmentation and volumetric analysis of the aortas in patients with infrarenal AAA[7,8,13,14]. Others added the measurements located at specific aortic areas, such as the AAA sac[10,11,16], and along all the aortic tree[6,15], but their analysis was again limited to extracting only maximum diameters and volumes measurements, without addressing the sealing zones. Kim et al.[17] proposed a segmentation approach that is based on Active Learning and a subsequent measurement algorithm. However, their work is restricted to a single institution and the segmentation necessitates manual intervention.

This narrow focus has led to the neglect of critical factors such as the quality of aortic branches and distal sealing zones, both of which are crucial for effective EVAR planning. Furthermore, there remains a notable gap in the automatic quantification of thrombus and calcifications in these regions, even though the literature highlights that iliac artery aneurysms develop in 10% to 40% of AAA cases.[18].

To overcome these limitations, this work introduces the *first comprehensive AI-driven solution* for AAA morphological features extraction. The tool, named BRAVE [Blood vessels Recognition and Aneurysms Visualization Enhancement], aims to facilitate EVAR planning with an easy, automatic and quick computation of all morphological features indicated in the new ESVS guidelines 2024[2]. These include proximal neck and AAA sac morphological features, but also aortic branches and proximal and distal sealing zones. The robustness and reliability of BRAVE were validated across diverse clinical settings by comparing its segmentations with those manually extracted by expert vascular surgeons. Additionally, a final comparison was performed between the morphological features extracted by BRAVE and those manually extracted using dedicated CE-marked commercial image processing software for EVAR. Results confirm accurate vessel identification, with correct segmentation in all cases compared to expert annotations in the external validation pre-CTAs dataset. Regarding the thrombus segmentation, the SegResNet network achieved an average Dice Similarity Coefficient of 0.96, demonstrating high accuracy, whereas for most anatomical regions the entire pipeline obtained a value above 0.85. Bland–Altman analysis showed that biases and limits of agreement were consistently below predefined clinical criteria, confirming the reliability of morphological features extraction.

To summarise, the main contributions of the paper are the following:

- *Comprehensive segmentation*: BRAVE segments not only the primary abdominal aorta but also identifies secondary vessels, often missed by existing methods, providing a complete picture of the vascular structure.
- *Volumetric analysis*: The pipeline performs advanced volumetric analysis of the AAA sac, quantifying thrombotic tissue and calcifications, which enhances surgical planning and decision-making.
- *Sealing Zones Identification*: BRAVE automatically identifies and analyzes the proximal and distal sealing zones, which are critical for successful EVAR procedures.
- *AI-driven automation*: The use of deep learning models (U-Net and SegResNet) and unsupervised algorithms enables fully automated processing, reducing the need for manual intervention and increasing the efficiency of the clinical workflow.
- *Generalizability*: Trained on a multi-center open access dataset, BRAVE is robust across varying CT protocols and patient populations, making it applicable in diverse clinical settings.

Materials and methods

The BRAVE pipeline

The BRAVE pipeline, as shown in Fig. 1, is an automatic tool designed for pre-CTA analysis in EVAR planning, comprising five consecutive steps that integrate deep learning and unsupervised machine learning algorithms. The process begins with Initial Segmentation using a pre-trained nnU-Net to identify key anatomical structures, including the aorta and iliac arteries. The Vessel Identification Algorithm (Algorithm 1) then identifies and segments secondary vessels of the infrarenal aorta. Next, the SegResNet network refines the segmentation, focusing on the thrombus within the aorta and common iliac arteries, a challenging task for traditional methods. The Areas Localization Algorithm (Algorithm 2) isolates areas of interest within the segmented images, accurately recognizing bifurcations and segmenting the AAA sac. Finally, the Morphological Features Extraction (Algorithm 3) module quantifies anatomical metrics, including thrombus and calcifications, according to the 2024 ESVS guidelines. The five consecutive steps are detailed in the following.

Initial segmentation

The first step performs an initial segmentation of the pre-CTAs to automatically identify mainly the aorta and the common iliac arteries, as well as external iliac arteries, and relevant anatomical structures as kidneys, vertebrae, common iliac veins, and the inferior vena cava, as Fig. 2 shows. This step uses a pretrained nnU-Net segmentation network that already proved effective in previous studies[19].

Vessels identification

A newly developed automated Vessels Identification Algorithm (VIA, Algorithm 1, Fig. 3) leverages initial segmentation results and anatomical relationships to identify secondary vessels branching from the infrarenal

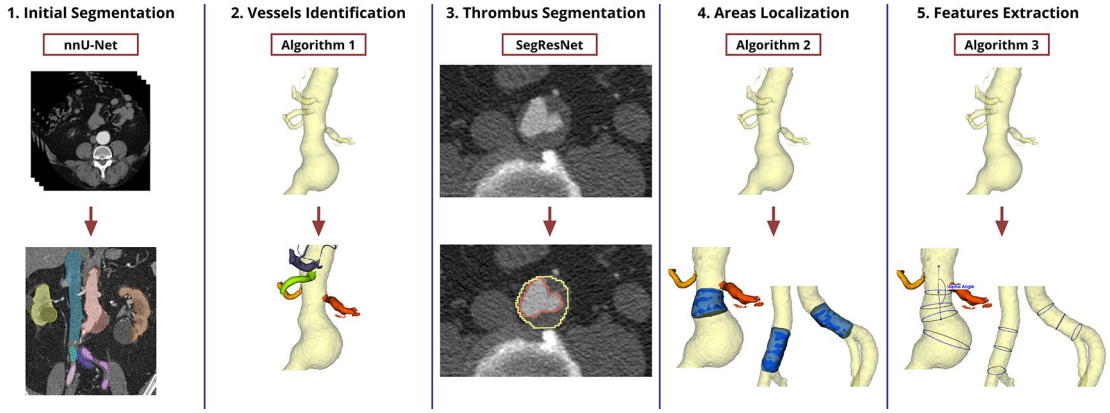

Fig. 1. Schematic representation of the BRAVE pipeline illustrating the 5 steps for processing an input pre-CTA. First, an initial segmentation of anatomical structures of interest was obtained through a nn-UNet, followed by a Vessel Identification Algorithm (Algorithm 1) which identifies and segments secondary vessels. Next, a SegResNet refines the segmentation of the aorta and iliac arteries (yellow vs red contours) and an Areas Localization Algorithm (Algorithm 2) isolates key anatomical parts for EVAR planning. Lastly a Morphological Features Extractor (Algorithm 3) estimates key features of the patient and generates a report. The figure was created using Photopea 5.4

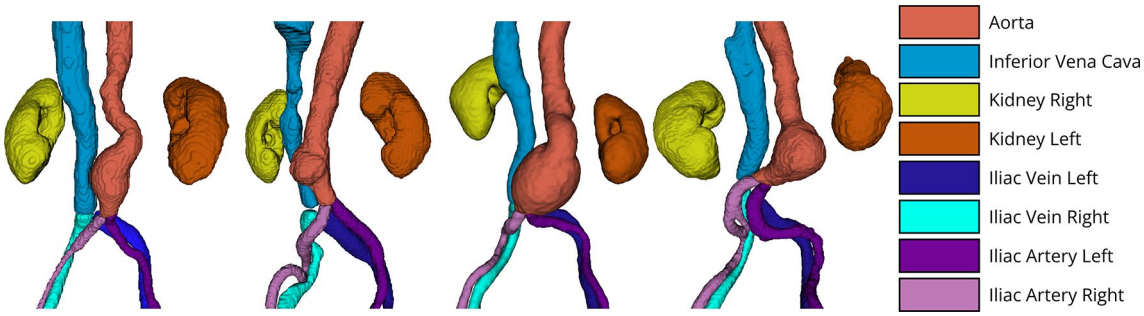

Fig. 2. Outputs produced by the nnU-Net in the first pipeline step for some selected patients. Each colour represents an anatomical structure of interest reported in the legend. The figure was created using Photopea 5.4 with 3D models generated in 3D Slicer 5.6.1.

aorta, including the renal arteries, celiac artery, superior mesenteric artery, and internal iliac arteries. These branches are segmented within a 5 cm radius from the centerline of the aorta and the common iliac arteries.

A flood-filling algorithm is first applied to the rough segmentation of the aorta and common iliac arteries using a 3D connected components approach with a neighborhood size value of 3. The algorithm divides high-intensity structures by applying an intensity threshold that is above the mean Hounsfield value of the vena cava, thereby ensuring the separation of arteries from veins. The remaining vessels, after excluding the aorta and common iliac arteries, are subsequently ranked using a non-linear aggregation function, specifically the Choquet integral. This approach combines information on the Euclidean distance in the physical space from the reference structures (e.g., kidneys) and the volumes to generate a score. A secondary vessel with the highest score for a key anatomical structure is then classified accordingly.

Thrombus segmentation

The third step performs a comprehensive thrombus segmentation within the aorta and common iliac arteries, a notably challenging task. Segmenting the thrombus in these areas is complicated. Indeed, the pretrained nnU-Net network struggles with this particular task due to the heterogeneity of the thrombus both within the same patient and across different patients and its proximity to structures of similar intensity. We thus developed a novel segmentation network, based on the SegResNet architecture, which is an encoder-decoder based convolutional network specifically trained for thrombotic tissue segmentation.

Areas localization

Subsequently, a dedicated algorithm, the Areas Localization Algorithm (ALA, Algorithm 2, Fig. 3), identifies all areas of interest within the segmented images. The process begins with the automatic detection of initial and terminal points, tracing the centerline between these points. An unsupervised algorithm separates bifurcated

Algorithm 1: Vessels Identification

Input: CT volume; segmentations of Kidneys, Aorta and Iliac Arteries
Output: segmentation of renal arteries, superior mesenteric artery, celiac and internal iliac arteries
1: Use Flood-filling algorithm (3D) with small neighborhood size starting on aorta at the level of the kidneys
2: Subtraction of the flood-filled segment with the segmentation of the Aorta and Iliac Arteries
3: Separate islands into separate structures
4: For every structure:
    4.1: Calculate distance from kidney left, kidney right, iliac artery left, iliac artery right
    4.2: Calculate volume
5: Aggregate volumes and distances into a normalized score using an aggregation function
6: **Return** segmentations with highest score on each key-structure

Algorithm 2: Areas Localization

Input: Refined segmentation of the aortic tree with centerlines
Output: Isolated areas of interest
1: Perform CPR on the centerlines of the aortic tree
2: Proximal Sealing Zone Isolation
    2.1: Delineation of lowest point of renal arteries
    2.2: Delineation of enlargement of the vessel (using a simple gradient-based check)
    2.3: Isolation of Proximal Sealing Zone
3: AAA Sac Isolation:
    3.1: Delineation of aorto-iliac bifurcation using Branch clipper tool
    3.2: Isolation of AAA sac
4: Distal Sealing Zones Isolation:
    4.1: Delineation of common-iliac bifurcations using Branch clipper tool
    4.2: Isolation of Common Iliac Arteries and distal sealing zones
5: **Return** new isolated segmentations

Algorithm 3: Morphological Features Extraction

Input: CT volume, demarcation points
Output: Morphological Features
1: Using information from demarcation points:
    1.1: Calculate diameters of sealing zones, lengths and angles
    1.2: Fit a two-component Gaussian Mixture Model (GMM) using sealing zones' walls HUs
    2.2: Classify voxels as thrombus or calcifications using the fitted GMM on sealing zones' walls
    2.3: Classify voxels as thrombus or calcifications using the fitted GMM on AAA sac
3: **Return** Extracted Morphological Features

Fig. 3. Pseudo-codes of unsupervised algorithms used in the automatic BRAVE's pipeline.

vascular segments into distinct branches based on their centerline model[20], thereby recognizing the aortic and common iliac bifurcations.

The aortic bifurcation is initially identified based on the segmentation performed with the nnU-Net. Then the SegResNet adds information about the thrombotic areas. At the end, the aortic bifurcation point can be identified with a better accuracy.

The nnU-Net's segmentation includes also the common iliac arteries but further isolation of the common iliac artery from the external iliac artery is still necessary. By applying Antiga's method, we effectively separate these components and accurately define the distal sealing zones, located just above the common iliac bifurcations.

This results in a complete segmentation of the AAA sac, including the lumen, proximal and distal sealing zones, and common iliac arteries.

Morphological features extraction

Finally the Morphological Features Extraction (MFE, Algorithm 3, Fig. 3) module automatically acquires all anatomical metrics, as outlined in the 2024 ESVS guidelines. All the single morphological features extracted are detailed in the Supplementary Table S1 online. Among these metrics, thrombus and calcifications within the proximal and distal sealing zones are quantified by an unsupervised clustering algorithm. While the sealing zones are segmented in prior steps, they do not specifically differentiate between thrombotic or calcified tissues. For this reason, additional quantification using clustering is necessary, as it allows for more accurate identification and quantification of these two tissue types within the sealing zones. The unsupervised clustering algorithm used is the Gaussian Mixture Model (GMM), which parametrized two normal distributions, one for each tissue type based on their Hounsfield numbers values with calcification having the distribution with the highest mean value, and thrombotic tissue, which has lower value.

The BRAVE pipeline was developed in Python 3.11.9 (https://www.python.org) using the Pytorch 2.3.0 (https://pytorch.org)[21], MONAI 1.3.0 (https://monai.io)[22], and VMTK 1.4.0 (http://www.vmtk.org)[23] libraries, integrated with the 3DSlicer 5.6.1 platform (https://www.slicer.org)[24,25] for visualisation and manual segmentation tasks. The SegResNet network was trained and validated on an NVIDIA RTX A5000 24 GB GPU, while the trained pipeline was used on a standard workstation.

Pipeline training and validation

The robustness and reliability of BRAVE were validated across diverse clinical settings, using pre-CTAs from publicly available datasets, representing a real-world dataset that generalises across different clinical institutions' imaging protocols.

The nnU-Net was pretrained on 1228 general purpose full body CT images from Zenodo[26], which included various scanners, acquisition sequences and institutions, as well as patients with and without AAAs. Since the network had already been extensively validated in a previous study[19], further validation was unnecessary.

A SegResNet was trained on 200 high-resolution cropped CTA images of AAA patients from a publicly available dataset[27], with both non-contrast and CTA images in high resolution (256×256 pixels) across 64 slices for each patient. The test set, including 20 additional cropped CTA images from the same repository, was used for thrombus segmentation validation. A detailed description of the SegResNet model, training pipeline, hyperparameter tuning, and relevant information is provided in the supplementary materials (Table S2), including model configuration, dataset and preprocessing, and evaluation metrics.

The entire pipeline was validated on an external set of 20 full abdomen pre-CTA scans from patients with AAA, collected from publicly available datasets[26,28–30].

Further details about the two validation procedures are described in the following.

Validation of thrombus segmentation

The thrombus within aorta and common iliac arteries is a complex tissue with significant variability in characteristics, such as porosity and calcification, both inter- and intra-patients. Its proximity to other abdominal structures with similar imaging intensities complicates the segmentation. Consequently, the pretrained nnU-Net network often fails to be accurate in this task. To overcome this, SegResNet was developed for precise segmentation of the aorta and the common iliac arteries, and their associated thrombus. The 220 pre-CTAs of AAA patients, available with the manually performed ground truth segmentation[27], were used for SegResNet training and testing, split in a 90%-10% ratio. Common metrics used to estimate the segmentation performance are the Dice Similarity Coefficient (DSC), Jaccard Index (JI), Sensitivity Index (SeI), Specificity Index (SpI) and Hausdorff Distance (HD). DSC is calculated as twice the number of pixels shared by both segmentations, divided by the total number of pixels in each mask. In contrast, JI is determined by dividing the intersection of the masks by their union. Sel is defined as the ratio of true positives to the sum of true positives and false negatives, whereas Spl is calculated as the ratio of true negatives to the sum of true negatives and false positives. Instead the HD measures the maximum distance between points on two surfaces, providing an upper bound on the discrepancy between them. It is commonly used to evaluate segmentation accuracy, particularly in 3D shape comparisons, by identifying the greatest distance from any point in one set to the nearest point in the other.

Validation of the full BRAVE pipeline

A comprehensive validation of the entire pipeline was performed on an additional set of 20 full abdomen pre-CTAs. This final validation process consisted of two steps. First, comparing the final automatic segmentations with manual segmentations performed by two expert vascular surgeons, using the segmentation tools of 3DSlicer platform on the CTA images slice by slice for each single patient. Second, validating the extraction of morphological features against those manually obtained using CE-marked software employed in clinical practice (3mensio Vascular 10.3 (https://www.3mensio.com), Pie Medical Imaging BV, Maastricht, NL).

The comparison between automated AI-based and manual segmentations (first step) was assessed using the previous metrics used for thrombus segmentation, i.e. DSC, JI, SeI, SpI and HD. Average performance across various anatomical regions (Table 1) was calculated to assess efficacy on each sub-segmentation task. Additionally, a general mean score was provided for overall capability evaluation.

In the second step, Bland–Altman analyses were performed on key morphological measurements (i.e. maximum/minimum diameters, angles and lengths) to assess agreement and identify potential biases or outliers. Following Giavarina D.[31], mean differences for each parameter were compared to clinically established a priori limits of maximum acceptable differences (Expected Limits of Agreement, ELoA, e.g. < 2 mm for proximal neck diameter) to evaluate feature extraction reliability. Specific analyses by extracted feature groups are detailed in Table 2.

Anatomical region	Dice similarity coefficient (DSC)	Jaccard index (JI)	Sensitivity index (Sel)	Hausdorff distance (HD)
Celiac Artery	0.91 ± 0.06	0.92 ± 0.05	0.91 ± 0.07	5.70 ± 6.82
Superior Mesenteric Artery	0.86 ± 0.11	0.88 ± 0.08	0.82 ± 0.16	6.52 ± 11.08
Left Renal Artery	0.90 ± 0.06	0.91 ± 0.05	0.93 ± 0.07	3.04 ± 2.68
Right Renal Artery	0.90 ± 0.07	0.91 ± 0.06	0.94 ± 0.05	2.21 ± 5.18
Proximal Neck	0.98 ± 0.01	0.98 ± 0.01	0.98 ± 0.02	3.08 ± 2.09
Proximal Neck Wall	0.79 ± 0.11	0.83 ± 0.07	0.73 ± 0.15	5.10 ± 7.16
AAA sac thrombus	0.97 ± 0.03	0.97 ± 0.03	0.98 ± 0.03	4.52 ± 5.02
AAA sac lumen	0.98 ± 0.01	0.98 ± 0.01	0.97 ± 0.02	5.34 ± 2.52
AAA sac calcification	0.60 ± 0.24	0.73 ± 0.13	0.69 ± 0.30	14.28 ± 7.50
Left Common Iliac Artery	0.96 ± 0.06	0.96 ± 0.05	0.97 ± 0.09	3.16 ± 2.82
Right Common Iliac Artery	0.97 ± 0.05	0.97 ± 0.04	0.98 ± 0.04	2.49 ± 3.14
Left Distal Sealing Zone	0.97 ± 0.04	0.97 ± 0.03	0.99 ± 0.02	2.18 ± 2.32
Left Distal Sealing Zone Wall	0.77 ± 0.14	0.82 ± 0.09	0.72 ± 0.13	4.54 ± 2.46
Right Distal Sealing Zone	0.96 ± 0.05	0.96 ± 0.04	0.99 ± 0.01	2.26 ± 3.13
Right Distal Sealing Zone Wall	0.74 ± 0.19	0.81 ± 0.10	0.70 ± 0.17	4.24 ± 2.44
Left Internal Iliac Artery	0.85 ± 0.12	0.88 ± 0.08	0.92 ± 0.11	6.19 ± 6.32
Right Internal Iliac Artery	0.87 ± 0.15	0.90 ± 0.09	0.93 ± 0.18	5.78 ± 9.64
Left External Iliac Artery	0.96 ± 0.02	0.96 ± 0.02	0.99 ± 0.01	3.00 ± 6.30
Right External Iliac Artery	0.95 ± 0.02	0.96 ± 0.02	0.97 ± 0.04	5.78 ± 10.62

Table 1. Evaluation of BRAVE's performance on various anatomical structures, against the surgeon's segmentations as the ground truth. Results are presented as mean ± standard deviation.

Morphological features group	Manual mean (SD)	Automatic mean (SD)	Bias mean difference	Upper LoA	Lower LoA	Expected limits of agreement (ELoA)	Percentage within ELoA
Proximal Neck diameters—mm	25.1	25.4	0.35	2.96	-2.26	2.0	82%
Maximum AAA sac diameters—mm	50.3	50.0	-0.37	2.04	-2.78	2.0	85%
Left Distal Sealing Zone diameters—mm	16.5	16.7	0.21	2.45	-2.03	2.0	93%
Right Distal Sealing Zone diameters—mm	16.3	16.4	0.12	2.79	-2.55	2.0	82%
All Lengths—mm	56.3	56.5	0.20	4.46	-4.05	3.0	76%
Alpha and Beta angles—°	30.5	29.6	-0.89	5.95	-7.74	5.0	89%
External Iliac arteries diameters—mm	8.8	7.8	-1.01	0.77	-2.78	2.0	80%
Minimum AAA Lumen and Max Bifurcation Diameters—mm	26.0	25.9	0.13	3.22	-2.97	2.0	73%
Suprarenal diameters—mm	25.2	25.8	0.57	2.66	-1.53	2.0	87%

Table 2. Results of the Bland–Altman analysis. Automatic and manual means together with bias mean differences are reported along with the upper and lower limits of agreements (LoAs) and the parameters percentage within a clinically established a priori limits of maximum acceptable differences (Expected Limits of Agreement, ELoA).

Additionally, a weighted Cohen's kappa statistic was used to assess the agreement on calcifications and thrombus in the sealing zones, while a correlation analysis evaluated the tortuosity indexes.

Results

Vessels identification

The accuracy of the VIA was evaluated by comparing the results with manual annotations provided by human experts. Among the 20 pre-CTAs of patients with AAA, all segmentations were correctly annotated by the automatic branch detection algorithm, without any misidentified artery. Figure 4 shows the final 3D reconstruction and mesh generation performed in 3DSlicer for a subset of patients.

Thrombus segmentation

The SegResNet network was evaluated on a test set comprising 20 pre-CTAs of patients with AAA. In Fig. 5, the manually created ground truth by an experienced cardiovascular radiologist and the automatically extracted thrombi from the aorta are superimposed on the pre-CTA to illustrate their overall concordance. The SegResNet achieves very accurate results on average, occasionally overestimating the thrombus in some slices (last column of Fig. 5A). According to the test set, the average values of the comparison metrics were 0.96 ± 0.002 for the

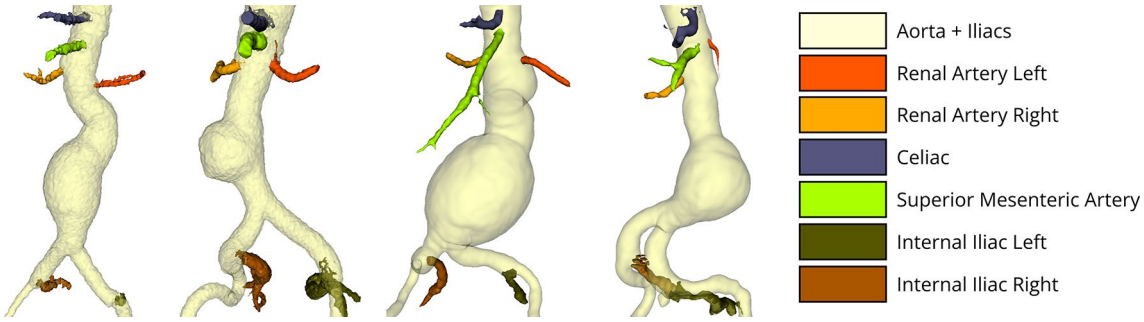

Fig. 4. Outputs generated by the Vessel Identification Algorithm in the second pipeline step for a selection of patients. The identified vessels are distinguished by specific colours according to the legend, while the aorta and iliacs (common iliac arteries including external iliac arteries) are depicted with partial transparency for reference. The figure was created using Photopea 5.4 with 3D models generated in 3D Slicer 5.6.1.

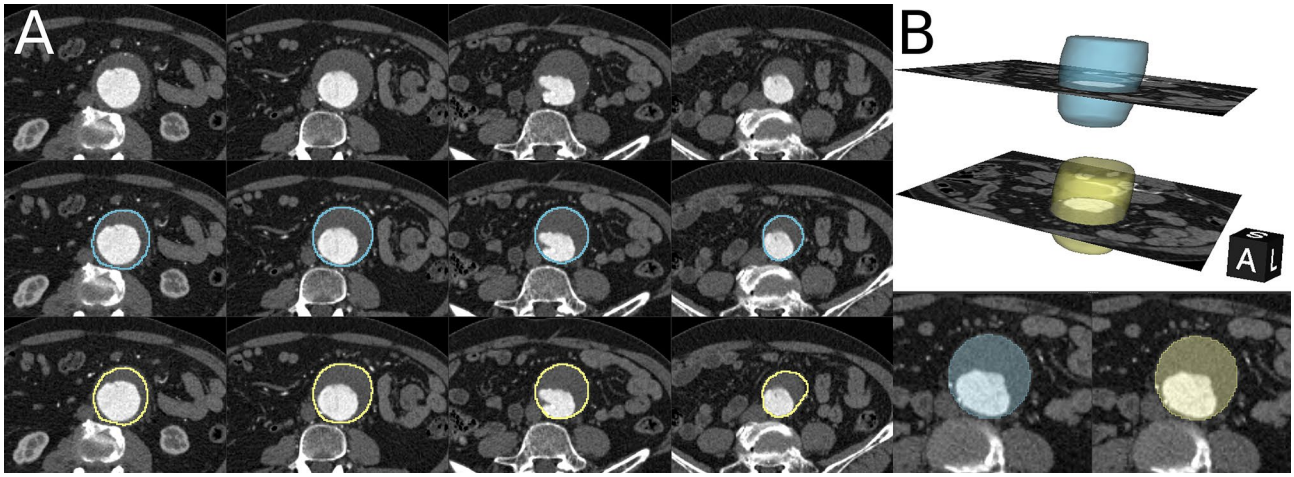

Fig. 5. Examples of segmentations produced by the SegResNet (yellow contours) compared with the respective ground truths (blue contours) (**A**), along with a 3D inspection (**B**).

DSC, 0.96 ± 0.002 for the JI, 0.98 ± 0.001 for SeI, and 0.99 ± 0.001 for SpI. Results clearly indicate that the model is adequately able to segment the aorta's thrombus.

Areas localization

In addition to aorta and common iliac arteries and their main branches recognised by previous algorithm, the AI-based tool identifies also the proximal and distal sealing zones, the AAA sac, encompassing the lumen, and common iliac arteries, as shown in Fig. 6. Results clearly indicate that the ALA is highly effective in accurately segmenting the entire AAA sac, which includes the lumen, proximal and distal sealing zones, as well as the common iliac arteries.

Overall pipeline

The analysis of automated AI-based segmentation in comparison to manual segmentation yielded the following average metric values across different anatomical regions, reported in Table 1. DSC, JI and SeI are above 0.85 with the exception of sealing walls (0.79, 0.77 and 0.74 for DSC, 0.83, 0.82 and 0.81 for JI, 0.73, 0.72 and 0.70 for SeI) and AAA sac calcification (0.60 for DSC, 0.73 for JI, 0.69 for SeI), due to the small extension of these anatomical structures, whereas SpI is always close to 1.00, due to the high number of voxels constituting the background of the images. Furthermore, the overall mean scores for all 20 patients were determined to be 0.88 for DSC, 0.91 for JI, 0.90 for SeI, and 0.99 for SpI. Highest HD values are associated with difficult structures to segment such as calcifications in the aneurysmal sac (14.28 mm), or secondary vessels that have several small-sized branches, internal iliac artery left and right (6.19 mm and 7.45 mm), superior mesenteric artery (6.52 mm) and celiac artery (5.70 mm); acceptable values for HD are associated with the remaining structures (between 2 and 5 mm).

The results highlighted the effectiveness of the AI-based approach for each sub-segmentation task, with average values reflecting the accurate and reliable tool's performance, also for thrombotic and aneurysmal common iliac arteries usually found in association with AAAs.

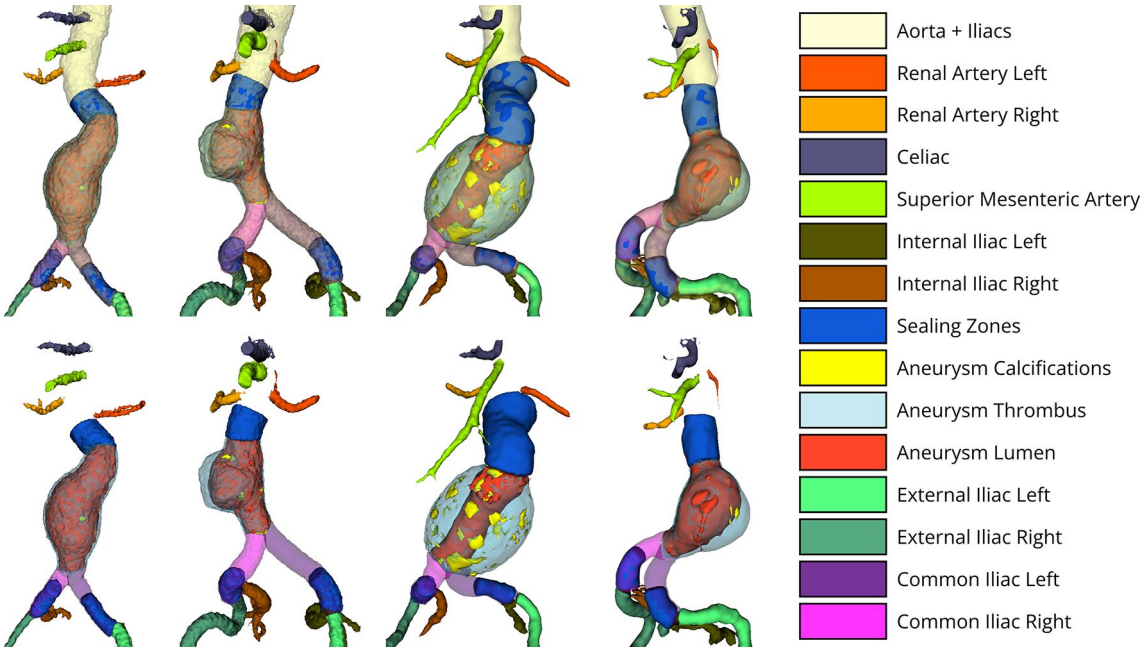

Fig. 6. Output generated by the Areas Localization Algorithm in the fourth pipeline step for a selection of patients. The first row displays also the aorta and iliac arteries (including the common and external iliac arteries) as a reference. The second row intentionally omits the aorta and iliacs to better highlight the results of the Areas Localization Algorithm, without being obscured by the white full aorto-iliac structure. The identified vessels and areas in the last row are indicated in the legend. The figure was created using Photopea 5.4 with 3D models generated in 3D Slicer 5.6.1

Biases and limits of agreement were consistently below predefined criteria, confirming the reliability of feature extraction, generally achieving over 80% performance, as shown in Bland–Altman plots for the main features extracted in Fig. 7 and summarized in Table 2. The "All lengths" group was at 76% due to variations in centerline generation algorithms, while "Minimum AAA Lumen and Max Bifurcation Diameters" was at 73% due to discrepancies in aortic bifurcation identification. The correlation between tortuosity indexes from both methods yielded a Pearson coefficient of 0.78 ($p < 0.001$), indicating strong agreement.

The unsupervised clustering algorithm assessed the proportions of calcification and thrombotic tissue in each sealing zone's wall. The weighted Cohen's kappa statistic showed substantial agreement between the algorithm and surgeons, with values of 0.77 for thrombotic tissue and 0.63 for calcification.

Additionally, as shown in Supplementary Table S3, the time taken for manual and automatic segmentation, as well as morphological feature extraction, is provided for the 20 full abdomen pre-CTAs.

Discussion

Accurate segmentation is crucial for successful EVAR. This study developed and validated BRAVE, an AI-driven software that enhances EVAR planning by efficiently computing key morphological features from pre-CTAs. The software aims to provide surgeons with an automated tool for EVAR planning, in line with the 2024 ESVS guidelines.

Previous studies offered tools that were not fully automated, lacked comprehensiveness, or provided partial analysis[6–15]. To address these limitations, a five-step automated pipeline has been developed, achieving unprecedented segmentation granularity, including accurate thrombus identification in the aorta and the iliac arteries. Segmenting thrombus in pre-CTAs is challenging due to the similarity in intensity values between thrombus and surrounding tissues, leading to mis-segmentation[32]. Traditional semi-automatic algorithms, such as level sets and graph cuts, often struggle with poorly contrasted boundaries, require significant user input, and rely on parameter tuning, limiting their clinical applicability[7]. BRAVE successfully addresses the task by employing a cascade of two networks, a pretrained nnU-Net for detecting the aorta and common iliac arteries and other critical organs followed by a SegResNet architecture for accurate thrombus segmentation, with an average DSC of 0.96, confirming its reliability. The accuracy of Vessels Identification and Areas Localization algorithms was validated by expert annotations, achieving perfect segmentation in a test set of 20 pre-CTAs of AAA patients. Additionally, the system accurately identifies sealing zones and the AAA sac, improving the segmentation of complex anatomical areas. The overall AI-based segmentation pipeline demonstrated strong performance, with DSC, JI, and SeI metrics above 0.85 for most regions, with only slight challenges in areas like aorto-iliac bifurcation and calcification on sealing walls or AAA sac.

The high HD values observed in the secondary vessels and in the AAA sac calcifications are a consequence of the challenges in the manual segmentation (e.g.: the difficulty in capturing tortuous vessels and the incomplete identification of calcified regions). Moreover, in the literature there are no available HD reference values of

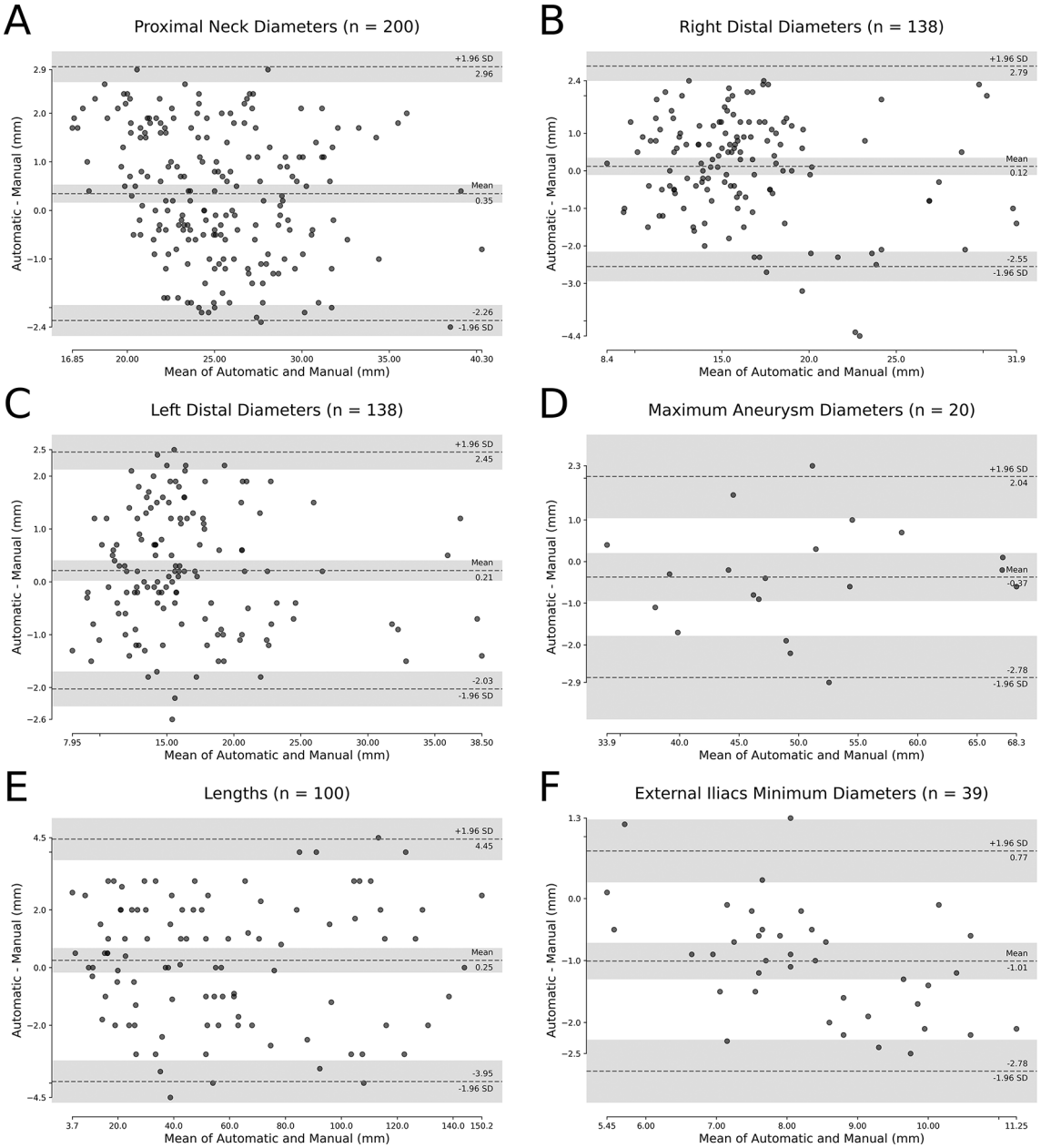

Fig. 7. Bland–Altman plots illustrating the agreement between the surgeons and the proposed system for a subset of features, i.e. Proximal Neck Diameters (**A**), Right (**B**) and Left (**C**) Distal Diameters, Maximum Aneurysm Diameters (**D**), Lengths (**E**) and Minimum Diameters of the External Iliacs (**F**).

secondary vessels and calcification for comparison. On the contrary, the HD values for the aorta's segments and common iliac arteries are in accordance with the results from the literature[15].

EVAR planning has mainly focused on addressing anatomical issues at the proximal neck, such as angulation, short necks, calcifications, and thrombus[33]. However, the equally important distal sealing zones present unique challenges that have been overlooked in the literature. An unsupervised clustering algorithm in BRAVE has been used to identify these areas, setting this research apart from existing literature by effectively addressing both the anatomical and technical constraints in their characterization[6–15,34,35]. This innovative approach enhances vascular surgeons' understanding of tissue properties, with confirmed agreement (Cohen's kappa statistics) for quantification of thrombus and calcification in the sealing zones, as suggested in the 2024 ESVS guidelines.

In addition, the AAA luminal volume is a significant risk factor for complications associated with EVAR. Previous studies indicate that volumetric analysis can more accurately assess changes in AAA and predict successful sac isolation after EVAR compared with traditional diameter measurements, affected by the difficulty in detecting shape changes, aortic tortuosity and high levels of interobserver variability[36,37]. These studies have highlighted the high reproducibility and reliability of volumetric assessment and, at the same time, the lack of clinically available software for volume calculations. The proposed automatic system addresses these aspects by

providing accurate volumetric segmentations and feature extractions in a time frame compatible with clinical workflows. An important outcome of this analysis was the substantial reduction in processing time, which directly addresses the common concern of time efficiency in daily clinical practice. By running the automatic approach in batch mode, the surgeon can fully dedicate their time to evaluating the results of segmentation and the automatically extracted measures, instead of spending time on tedious, time-consuming, and monotonous tasks. This shift allows for more efficient use of the surgeon's time, greatly improving clinical workflows.

Overall, the AI-driven tool successfully extracted all morphological features in accordance with the 2024 ESVS guidelines, demonstrating minimal bias and adhering to agreement limits approximately 80% of the time. These findings are consistent with the results of recent validation studies[15,16] for what concerns infrarenal aortic diameter measurements. By analyzing the Bland–Altman plots, compared to most recent work of Kim et al.[17], the measurements of maximum diameter and those at the proximal neck and sealing zones, this study achieves limits of agreement that are about 1 mm and 5 mm better for the lengths on average. For other morphological features, such as angles or tissue characterization, no comparisons were available as BRAVE is the first automated approach capable of extracting them.

Despite variability from CTA scan resolution and statistical factors, the differences between automatic and manual feature extraction remain within clinically strict a priori criteria. The observed deviations were primarily due to incorrect measurements related to uncorrected automatic segmentation of the aortic-iliac region. This misidentification occurred either from challenges in distinguishing the aneurysm from surrounding structures—such as duodenum or intestinal loops or adjacent vasculature like the inferior mesenteric artery—due to the similar pixel intensities, or from an inability to precisely identify key anatomical landmarks, such as aortic bifurcation or secondary blood vessels bifurcations. These aspects were also identified as the main reasons for discrepancies in recent external validation of automatic tools for infrarenal maximum aortic aneurysm diameter estimation[16].

This limited deviation from the a priori rigorous criteria is largely compensated by the significant benefits of automating the segmentation process and morphological features extraction. These features are essential in clinical EVAR planning, enabling automated selection of aortic SG for the surgeon. Currently, this selection relies solely on the instructions for use (IFU) provided by the manufacturer. Future research may explore if the automatically-extracted features can be used to address whether a particular SG, not strictly adhering to the IFUs, could still be suitable, aiding surgeons in solving complex problems.

The study's primary limitation is the small sample size used for the final tool validation. Online searches were conducted to identify appropriate full abdomen CTA scans that must include the entire abdomen of the patient, ensuring that both the iliac and celiac arteries are visible, the patients have an infrarenal abdominal aneurysm, and the patients are eligible for EVAR. Only a limited number of CTA scans were identified that satisfied these criteria. Furthermore, the annotation of the dataset required a tedious process of manual segmentations and complete EVAR planning by expert surgeons for all of the full abdomen pre-CTA scans that were identified, an additional evidence of the importance of the proposed automatic system. On the other hand, using pre-CTAs from online repositories enhanced the AI software's robustness and reliability across clinical settings. Indeed, this approach created a dataset that mirrors real-world conditions, incorporating diverse imaging protocols from various healthcare institutions. By integrating scans from multiple environments, the AI adapted to different techniques and equipment, managing discrepancies for practical robustness. The use of accessible repositories provided a diverse range of cases, crucial for training the AI to effectively analyse and interpret pre-CTAs, improving its generalisation and predictive accuracy in new scenarios.

Additionally, BRAVE creates high-quality 3D models of AAAs and surrounding vasculature, crucial for EVAR planning, sizing SG, and personalised clinical decisions. These models obtained automatically from BRAVE can also be used for AAA growth simulation, computational fluid dynamics (CFD) analysis, shape assessment, and development of risk assessment algorithms, with the added potential for 3D printing to create patient-specific anatomical models.

In summary, the findings show that the proposed tool allows to spare entirely the vascular surgeons' time needed for segmentation and morphological features extraction for EVAR planning. The solution offers a detailed pre-planning analysis for EVAR and has proven to be accurate, robust and reliable.

Interpretability is a critical component for clinical adoption. The BRAVE pipeline provides rich information about how morphological features are computed, from detailed segmentation of the anatomical structure to highlights on the most important landmarks within the CT-scan. Each of these elements can be evaluated by the surgeon, enhancing the understanding of the model's outputs.

It is important to emphasize that BRAVE serves as a support to the vascular surgeon's activities in the EVAR planning, rather than a complete replacement, enhancing efficiency without compromising clinical precision. The system is designed to be easily integrated into existing preoperative workflows by simply loading CTA images, which are routinely available before EVAR procedures. It offers automated insights in an interpretable format, with the surgeon maintaining full control over the results and being able to revise them as needed, ensuring that clinical decision-making remains under the physician's discretion. This approach allows the tool to act as a supportive aid rather than a replacement for the vascular surgeon's expertise. However, successful implementation in clinical settings will depend on addressing regulatory requirements and ensuring the tool's robustness through additional investigations.

Conclusion

This research developed and validated BRAVE (Blood vessels Recognition and Aneurysms Visualization Enhancement), a fully automated AI software designed to enhance EVAR planning. BRAVE efficiently extracts various morphological features, such as thrombus and calcifications, demonstrating reliability across clinical settings and significantly reducing planning time for vascular surgeons. By automating morphological analysis

and streamlining pre-CTA evaluations, the software aims to standardise results, improving the efficiency and accuracy of EVAR planning, ultimately benefiting both patients and healthcare professionals.

Data availability

Data and derived statistical analyses are available from the corresponding author upon request.

Received: 13 January 2025; Accepted: 28 April 2025
Published online: 12 May 2025

References

1. Patel, R., Sweeting, M., Powell, J. & Greenhalgh, R. Endovascular versus open repair of abdominal aortic aneurysm in 15-years' follow-up of the UK endovascular aneurysm repair trial 1 (EVAR trial 1): A randomised controlled trial. *The Lancet.* **388**, 2366–2374 (2016).
2. Wanhainen, A. et al. Editor's choice—European Society for Vascular Surgery (ESVS) 2024 clinical practice guidelines on the management of abdominal Aorto-iliac artery aneurysms. *Eur. J. Vasc. Endovasc. Surg.* **67**, 192–331 (2024).
3. Hallett, R., Ullery, B. & Fleischmann, D. Abdominal aortic aneurysms: Pre-and post-procedural imaging. *Abdom. Radiol.* **43**, 1044–1066 (2018).
4. Fabre, D., Postiglione, T. & Haulon, S. AI, Automation, and aortic aneurysm care. *Endovasc. Today.* https://evtoday.com/articles/2023-mar/ai-automation-and-aortic-aneurysm-care
5. Cercenelli, L. et al. EVAR-eaSE: An easy-to-use software for planning sac embolization in endovascular aneurysm repair procedure. *Appl. Sci.* **10**, 6252 (2020).
6. Adam, C. et al. Pre-surgical and post-surgical aortic aneurysm maximum diameter measurement: Full automation by artificial intelligence. *Eur. J. Vasc. Endovasc. Surg.* **62**, 869–877 (2021).
7. Lareyre, F. et al. A fully automated pipeline for mining abdominal aortic aneurysm using image segmentation. *Sci. Rep.* **9**, 13750 (2019).
8. López-Linares, K. et al. Fully automatic detection and segmentation of abdominal aortic thrombus in post-operative CTA images using Deep Convolutional Neural Networks. *Med. Image Anal.* **46**, 202–214 (2018).
9. Fantazzini, A. et al. 3D automatic segmentation of aortic computed tomography angiography combining multi-view 2D convolutional neural networks. *Cardiovasc. Eng. Technol.* **11**, 576–586 (2020).
10. Brutti, F. et al. Deep learning to automatically segment and analyze abdominal aortic aneurysm from computed tomography angiography. *Cardiovasc. Eng. Technol.* **13**, 535–547 (2022).
11. Caradu, C., Spampinato, B., Vrancianu, A. M., Berard, X. & Ducasse, E. Fully automatic volume segmentation of infrarenal abdominal aortic aneurysm computed tomography images with deep learning approaches versus physician controlled manual segmentation. *J. Vasc. Surg.* **74**, 246-256.e6 (2021).
12. Huang, L. et al. Deep learning techniques for imaging diagnosis and treatment of aortic aneurysm. *Front. Cardiovasc. Med.* **11**, 1354517 (2024).
13. Siriapisith, T., Kusakunniran, W. & Haddawy, P. A retrospective study of 3D deep learning approach incorporating coordinate information to improve the segmentation of pre-and post-operative abdominal aortic aneurysm. *PeerJ Comput. Sci.* **8**, e1033 (2022).
14. Abdolmanafi, A., Forneris, A., Moore, R. & Di Martino, E. Deep-learning method for fully automatic segmentation of the abdominal aortic aneurysm from computed tomography imaging. *Front. Cardiovasc. Med.* **9**, 1040053 (2023).
15. Postiglione, T. et al. Multicentric clinical evaluation of a computed tomography-based fully automated deep neural network for aortic maximum diameter and volumetric measurements. *J. Vasc. Surg.* **79**, 1390-1400.e8 (2024).
16. Hatzl, J. et al. External validation of fully-automated infrarenal maximum aortic aneurysm diameter measurements in computed tomography angiography scans using artificial intelligence (PRAEVAorta 2). *J. Endovasc. Ther.* https://doi.org/10.1177/15266028241295563 (2024).
17. Kim, T., On, S., Gwon, J. G. & Kim, N. Computed tomography-based automated measurement of abdominal aortic aneurysm using semantic segmentation with active learning. *Sci. Rep.* **14**, 8924 (2024).
18. Zhang, J. et al. Incidence and management of iliac artery aneurysms associated with endovascular treatment of juxtarenal and thoracoabdominal aortic aneurysms. *J. Vasc. Surg.* **72**, 1360–1366 (2020).
19. Wasserthal, J. et al. TotalSegmentator: Robust segmentation of 104 anatomic structures in CT images. *Radiol. Artif. Intell.* **5**, e230024 (2023).
20. Antiga, L. & Steinman, D. A. Robust and objective decomposition and mapping of bifurcating vessels. *IEEE Trans. Med. Imaging* **23**, 704–713 (2004).
21. Paszke, A. et al. Pytorch: An imperative style, high-performance deep learning library. *Adv. Neural. Inf. Process. Syst.* **32**, 8024–8035 (2019).
22. Cardoso, M. *et al.* Monai: An open-source framework for deep learning in healthcare. http://arXiv.org/abs/2211.02701 (2022).
23. Izzo, R., Steinman, D., Manini, S. & Antiga, L. The vascular modeling toolkit: A python library for the analysis of tubular structures in medical images. *J. Open Source Softw.* **3**, 745 (2018).
24. Kikinis, R., Pieper, S.D., Vosburgh, K.G. 3D slicer: A platform for subject-specific image analysis, visualization, and clinical support. In *Intraoperative Imaging and Image-Guided Therapy* 277–289. (Springer, New York, 2014).
25. Fedorov, A. et al. 3D Slicer as an image computing platform for the Quantitative Imaging Network". *Magn. Reson. Imaging* **30**, 1323–1341 (2012).
26. Wasserthal, J. Dataset with segmentations of 117 important anatomical structures in 1228 CT images. Zenodo https://doi.org/10.5281/ZENODO.6802613 (2023).
27. Siriapisith, T., Kusakunniran, W. & Haddawy, P. A 3D deep learning approach incorporating coordinate information to improve the segmentation of pre-and post-operative abdominal aortic aneurysm. Figshare https://doi.org/10.6084/M9.FIGSHARE.19090052.V1 (2022).
28. Wilson, N. M., Ortiz, A. K. & Johnson, A. B. The vascular model repository: a public resource of medical imaging data and blood flow simulation results. *J. Med. Devices* **7**, 040923 (2013).
29. Radl, L. et al. Aortic Vessel Tree (AVT) CTA datasets and segmentations. Figshare https://doi.org/10.6084/M9.FIGSHARE.14806362.V1 (2022).
30. Clark, K. et al. The Cancer Imaging Archive (TCIA): Maintaining and Operating a Public Information Repository. *J. Digit. Imaging* **26**, 1045–1057 (2013).
31. Giavarina, D. Understanding Bland Altman analysis. *Biochemia Medica* **25**, 141–151 (2015).
32. Hwang, B. et al. Automatic detection and segmentation of thrombi in abdominal aortic aneurysms using a mask region-based convolutional neural network with optimized loss functions. *Sensors* **22**, 3643 (2022).
33. De Vries, J.-P.P.M. The proximal neck: the remaining barrier to a complete EVAR world. *Semin. Vasc. Surg.* **25**, 182–186 (2012).

34. Kyriakou, F., Dempster, W. & Nash, D. A methodology to quantify the geometrical complexity of the abdominal aortic aneurysm. *Sci. Rep.* **9**, 17379 (2019).
35. Raffort, J. et al. Artificial intelligence in abdominal aortic aneurysm. *J. Vasc. Surg.* **72**, 321-333.e1 (2020).
36. Kouvelos, G., Volakakis, G., Dakis, K., Spanos, K. & Giannoukas, A. The role of aortic volume in the natural history of abdominal aortic aneurysms and post-endovascular aortic aneurysm repair surveillance. *J. Clin. Med.* **13**, 193 (2023).
37. Oliveira-Pinto, J. et al. Total luminal volume predicts risk after endovascular aneurysm repair. *Eur. J. Vasc. Endovasc. Surg.* **59**, 918–927 (2020).

Author contributions

E.R. and D.R. contributed to conceptualization, methodology, software, validation, formal analysis, data curation, writing—original draft, writing—review & editing, and visualization.A.T. and A.P. contributed to conceptualization, investigation, resources, data curation, writing— original draft, writing—review & editing, supervision, project administration, and funding acquisition. S.A. and I.R. contributed to manual segmentation and manual measurements.S.B. contributed to supervision and project administration.All authors: manuscript review and editing, critical revision for important intellectual content.

Funding

Funded by the European Union. Views and opinions expressed are however those of the author(s) only and do not necessarily reflect those of the European Union or the European Health and Digital Executive Agency (HaDEA). Neither the European Union nor the granting authority can be held responsible for them. Grant Agreement No. 101120763 - TANGO.

Declarations

Competing interests

The authors declare no competing interests.

Additional information

Supplementary Information The online version contains supplementary material available at https://doi.org/10.1038/s41598-025-00484-7.

Correspondence and requests for materials should be addressed to E.R.